Title

Phonon-Assisted Ballistic Current from First-Principles Calculations

Journal

Physical Review Letters, 126(17)

ISSN

0031-9007

Authors

Dai, Zhenbang

Schankler, Aaron M

Gao, Lingyuan

et al.

Publication Date

2021-04-30

DOI

10.1103/physrevlett.126.177403

Peer reviewed

Phonon-Assisted Ballistic Current from First-Principles Calculations

Zhenbang Dai,[1,†] Aaron M. Schankler,[1,†] Lingyuan Gao,[1] Liang Z. Tan,[2] and Andrew M. Rappe[1,*]
[1]*Department of Chemistry, University of Pennsylvania, Philadelphia, Pennsylvania 19104–6323, USA*
[2]*Molecular Foundry, Lawrence Berkeley National Laboratory, Berkeley, California 94720, USA*

The bulk photovoltaic effect (BPVE) refers to current generation due to illumination by light in a homogeneous bulk material lacking inversion symmetry. In addition to the intensively studied shift current, the ballistic current, which originates from asymmetric carrier generation due to scattering processes, also constitutes an important contribution to the overall kinetic model of the BPVE. In this Letter, we use a perturbative approach to derive a formula for the ballistic current resulting from the intrinsic electron-phonon scattering in a form amenable to first-principles calculation. We then implement the theory and calculate the ballistic current of the prototypical BPVE material $BaTiO_3$ using quantum-mechanical density functional theory. The magnitude of the ballistic current is comparable to that of the shift current, and the total spectrum (shift plus ballistic) agrees well with the experimentally measured photocurrents. Furthermore, we show that the ballistic current is sensitive to structural change, which could benefit future photovoltaic materials design.

The bulk photovoltaic effect (BPVE) is the phenomenon of photocurrent generation in a homogeneous material that lacks inversion symmetry [1,2]. Compared to traditional photovoltaic devices with a *p-n* junction to separate electron-hole pairs, where the power conversion efficiency cannot go beyond the Shockley-Queisser limit [3], the BPVE can generate large short-circuit photocurrent and above-band gap photovoltage, thus potentially surpassing the efficiency limit of conventional solar cells [4,5].

Shift current, which is a purely quantum mechanical effect, is considered to be one of the dominant mechanisms of the BPVE. The shift current results from the coherent evolution of a quantum wave packet; a net current is generated by a real-space shift of excited electrons under illumination. The shift current has been extensively studied analytically and is also readily obtained from first-principles calculations based on electronic structure [6–10]. This enables *ab initio* study of the shift current response of a wide variety of materials, including those in Refs. [11–14]. Though no overarching design rules have been established, previous studies have established links between shift current response and wave function delocalization and polarization [4,15–17]. Although the shift current mechanism is a major component of the BPVE, our recent first-principles study shows that it cannot fully account for the experimental photocurrent spectrum of $BaTiO_3$ [18]. Indeed, unlike shift current which is a purely excitation theory, kinetic processes including the relaxation and recombination of photoexcited carriers are often not taken into account. Therefore, other mechanisms related with kinetic processes must also be studied for a full understanding of the BPVE.

Ballistic current, which is a current based on carrier transport, results from asymmetric occupation of carriers at momentum $\mathbf{k}$ and $-\mathbf{k}$ [19], and it is viewed as a dominant mechanism for the BPVE [20–23]. In the absence of inversion symmetry, the occupation is determined by different asymmetric scattering processes, including scattering from defects, electron-hole interactions, and the electron-phonon interactions [19,21,24,25], whereas for magnetic systems which break time-reversal symmetry, the asymmetric momentum distribution can still exist without these scattering mechanisms [1,21,26]. We will focus on materials with time-reversal symmetry. Among these asymmetric scattering processes, electron-phonon scattering is an intrinsic mechanism present regardless of the quality of the material, and it will be strongly influenced by temperature. As revealed in Ref. [27], both ballistic current and shift current are significant mechanisms for BPVE in $Bi_{12}GeO_{20}$. Although there are several previous studies calculating ballistic current, they are based on few-band models, and approximations are usually made assuming that only certain regions of the Brillouin zone contribute [21–24]. Therefore, to establish the importance of ballistic current for real materials, it is imperative to have a study based on the full electronic structure and phonon dispersion.

In this Letter, we perform a first-principles study of the ballistic current due to electron-phonon scattering (referred to here simply as the ballistic current). To the best of our knowledge, no such calculation has yet been reported. Following previous work [19,24], we take the electron-phonon coupling as the source of scattering and derive the asymmetric carrier generation rate using a Kubo formula. With the developed *ab initio* Frölich electron-phonon interaction, the carrier generation rate can be calculated in an *ab initio* way. With the rate and band velocities, current can be calculated according to the Boltzmann

transport equation. We compare our results with theoretically calculated shift current and also with the experimentally measured photocurrent of $BaTiO_3$ [18,28]. We also explore the ballistic current in different crystal structures of this material, and we find that the magnitude of ballistic current can vary significantly.

Based on the Boltzmann transport equation, the phonon-assisted ballistic current can be expressed as

$$j^{\alpha\beta,\gamma}(\omega) = 2e\tau_0 \sum_{cv\mathbf{k}} \Gamma^{\alpha\beta,\mathrm{asym}}_{cv,\mathbf{k}}(\omega)[v^{e,\gamma}_{c\mathbf{k}} - v^{e,\gamma}_{v\mathbf{k}}], \tag{1}$$

where $\Gamma^{\alpha\beta,\mathrm{asym}}_{cv,\mathbf{k}}(\omega) = \frac{1}{2}[\Gamma^{\alpha\beta}_{cv,\mathbf{k}}(\omega) - \Gamma^{\alpha\beta}_{cv,-\mathbf{k}}(\omega)]$ is the asymmetric carrier generation rate for an electron-hole pair (c, v) at $\mathbf{k}$, e is the electron charge, τ_0 is the momentum relaxation time, and $\mathbf{v}^e_{c\mathbf{k}}$ ($\mathbf{v}^e_{v\mathbf{k}}$) is the electron (hole) velocity obtained from band derivatives. The leading factor of 2 is for spin degeneracy. The central quantity that needs to be evaluated is the asymmetric carrier generation rate, and it is derived below.

Adopting the velocity gauge $\mathbf{E} = -(\partial\mathbf{A}/\partial t)$ and taking the electron-photon interaction as $\hat{H}_{e-\mathrm{photon}} = (e/m)\hat{\mathbf{P}}\cdot\hat{\mathbf{A}}$, from linear response theory [29,30], the average power delivered by monochromatic light of frequency ω to the system during one period of oscillation is

$$W = -2\omega \mathrm{Im}[\chi^{\alpha\beta}(\omega)]\left(\frac{e}{m\omega}\right)^2 E_\alpha(\omega)E_\beta(\omega), \tag{2}$$

where $\chi^{\alpha\beta}(\omega)$ is the rank-two response function in the presence of $\mathbf{E}$ field with Greek letters denoting its components, e and m are the electron charge and mass, and $E_\alpha(\omega)$ is the amplitude of the electric field, whose frequency dependence will be taken implicitly hereafter. Considering that each photon absorbed will be converted to an electron and hole, [25], the overall carrier generation rate $\Gamma^{\alpha\beta}(\omega)$ can then be written as

$$\Gamma^{\alpha\beta}(\omega) = \frac{W}{\hbar\omega} = -\frac{2}{\hbar}\mathrm{Im}[\chi^{\alpha\beta}(\omega)]\left(\frac{e}{m\omega}\right)^2 E_\alpha E_\beta. \tag{3}$$

According to the Kubo formula, the response function is related to the retarded momentum-momentum correlation function

$$\begin{aligned}\chi^{\alpha\beta}(\omega) &= \frac{1}{\hbar} C^R_{\hat{P}^\alpha\hat{P}^{\dagger\beta}}(\omega) \\ &= -\frac{i}{\hbar}\int_{-\infty}^{+\infty} dt e^{-i\omega t}\Theta(t)\langle[\hat{P}^\alpha(t), \hat{P}^{\dagger\beta}(0)]\rangle. \end{aligned}\tag{4}$$

Here, the brackets $\langle\cdot\rangle$ indicate an equilibrium average with respect to the total Hamiltonian that includes any extra interaction $\hat{H}'$, which in our case is the electron-phonon interaction, and the momentum operators are in the Heisenberg picture. To evaluate $\chi^{\alpha\beta}(\omega)$, we first calculate the imaginary-time (Matsubara) correlation function in its second quantization form with Bloch states as the basis:

$$\begin{aligned}\chi^{\alpha\beta}_T(i\omega_n) = -\frac{1}{\hbar}\sum_{\mathbf{k}\mathbf{k}'cc'vv'} &\langle v\mathbf{k}|\hat{P}^\alpha|c\mathbf{k}\rangle\langle c'\mathbf{k}'|\hat{P}^\beta|v'\mathbf{k}'\rangle \\ \times \int_0^{\hbar/k_BT} d\tau e^{i\omega_n\tau}\langle \hat{T}_\tau \hat{c}^\dagger_{v\mathbf{k}}(\tau)\hat{c}_{c\mathbf{k}}(\tau)\hat{c}^\dagger_{c'\mathbf{k}'}(0)\hat{c}_{v'\mathbf{k}'}(0)\rangle,\end{aligned}\tag{5}$$

where $c(c')$ and $v(v')$ are band indices for conduction and valence bands, respectively, $\mathbf{k}, \mathbf{k}'$ are crystal momenta, and $1/k_BT$ reflects the influence of temperature [31]. The retarded and Matsubara correlation functions can be related through analytical continuation: $\chi^{\alpha\beta}(\omega) = \chi^{\alpha\beta}_T(i\omega_n \to \omega + i0^+)$, where 0^+ is a infinitesimal positive number. In Eq. (5), two conditions hold: first, due to Pauli exclusion, transitions are only allowed from occupied valence bands to unoccupied conduction bands; also the population of electrons in a semiconductor is not significantly influenced by temperature. Second, because of the negligible momentum carried by photons, only vertical transitions are allowed. From Eq. (5), it can be seen that the carrier generation rate $\Gamma^{\alpha\beta}(\omega)$ can be decomposed into components from various $\mathbf{k}$ points and electron-hole pairs: $\Gamma^{\alpha\beta}(\omega) = \sum_{cv\mathbf{k}}\Gamma^{\alpha\beta}_{cv,\mathbf{k}}(\omega)$, and we only consider the asymmetric scatterings $\Gamma^{\alpha\beta}_{cv,\mathbf{k}}(\omega) \neq \Gamma^{\alpha\beta}_{cv,-\mathbf{k}}(\omega)$ as the contribution to net current. Without any other interaction, Eq. (5) corresponds to Fermi's golden rule, and this is a symmetric excitation which does not generate any current.

Therefore, we calculate the carrier generation rate in the presence of electron-phonon coupling, which will impose the influence of temperature. By introducing the Frölich e-ph Hamiltonian as [29,31,32]

$$\hat{H}'_{e-\mathrm{phonon}} = \sum_{\mu nn'}\sum_{\mathbf{k}\mathbf{k}'} g^{nn'}_{\mu\mathbf{k}\mathbf{k}'}\hat{c}^\dagger_{n'\mathbf{k}'}\hat{c}_{n\mathbf{k}}\hat{\Phi}^\mu_{\mathbf{k}-\mathbf{k}'}, \tag{6}$$

where $\hat{\Phi}^\mu_{\mathbf{q}} = \hat{a}^\mu_{\mathbf{q}} + \hat{a}^{\mu\dagger}_{-\mathbf{q}}$ is the phonon field operator, $\hat{a}^\mu_{\mathbf{q}}(\hat{a}^{\mu\dagger}_{\mathbf{q}})$ are the phonon annihilation(creation) operators, and $g^{nn'}_{\mu\mathbf{k}\mathbf{k}'}$ is the electron-phonon coupling matrix, we perform a perturbative expansion using a Feynman diagrammatic approach. The lowest-order nonzero contribution is second order, illustrated as three different diagrams in Fig. 1. As shown in the Supplemental Material [33], the processes of Fig. 1(b)

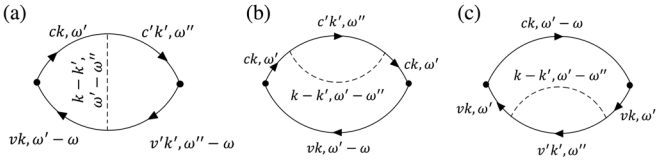

FIG. 1. Three different Feynman diagrams for the second-order expansion of the momentum-momentum correlation function with the electron-phonon coupling as the perturbation. Only diagram (a) will contribute to asymmetric scattering.

and 1(c) are symmetric scattering, and only Fig. 1(a) contributes to asymmetric scattering. By applying Feynman rules on Fig. 1(a) and performing analytical continuation, we can find the second-order correction to the carrier generation rate $\Delta\Gamma^{\alpha\beta}_{cv,\mathbf{k}}(\omega)$. Finally, we use relations that are satisfied for materials with time-reversal symmetry

$$\begin{aligned}\langle v,-\mathbf{k}|\hat{P}^{\alpha}|c,-\mathbf{k}\rangle &= -\langle v,\mathbf{k}|\hat{P}^{\alpha}|c,\mathbf{k}\rangle^{*}\\ g^{nn'}_{\mu-\mathbf{k}-\mathbf{k}'} &= (g^{nn'}_{\mu\mathbf{k}\mathbf{k}'})^{*}\end{aligned} \tag{7}$$

to write the asymmetric carrier generation rate:

$$\begin{aligned}\Gamma^{\alpha\beta,\mathrm{asym}}_{cv,\mathbf{k}}(\omega) &= \frac{1}{2}\left(\Delta\Gamma^{\alpha\beta}_{cv,\mathbf{k}}(\omega)-\Delta\Gamma^{\alpha\beta}_{cv,-\mathbf{k}}(\omega)\right)\\ &= \frac{2}{\hbar}\left(\frac{\pi e}{m\omega}\right)^{2}E_{\alpha}E_{\beta}\sum_{c'v'\mathbf{k}'\mu}\mathrm{Im}[\langle v\mathbf{k}|\hat{P}^{\alpha}|c\mathbf{k}\rangle\langle c'\mathbf{k}'|\hat{P}^{\beta}|v'\mathbf{k}'\rangle g^{cc'}_{\mu\mathbf{k}\mathbf{k}'}g^{v'v}_{\mu\mathbf{k}'\mathbf{k}}]\\ &\times\Bigg\{(N_{\mathbf{q}}+1)\Bigg[\delta(E_{c\mathbf{k}}-E_{v\mathbf{k}}-\hbar\omega)\delta(E_{c'\mathbf{k}'}-E_{v'\mathbf{k}'}-\hbar\omega)\left(\mathcal{P}\frac{1}{E_{c'\mathbf{k}'}-E_{c\mathbf{k}}+\hbar\omega_{\mathbf{q}}}+\mathcal{P}\frac{1}{E_{v\mathbf{k}}-E_{v'\mathbf{k}'}+\hbar\omega_{\mathbf{q}}}\right)\\ &+\delta(E_{c\mathbf{k}}-E_{v\mathbf{k}}-\hbar\omega)\mathcal{P}\frac{1}{E_{c'\mathbf{k}'}-E_{v'\mathbf{k}'}-\hbar\omega}\left(\delta(E_{c'\mathbf{k}'}-E_{c\mathbf{k}}+\hbar\omega_{\mathbf{q}})+\delta(E_{v\mathbf{k}}-E_{v'\mathbf{k}'}+\hbar\omega_{\mathbf{q}})\right)\\ &+\mathcal{P}\frac{1}{E_{c\mathbf{k}}-E_{v\mathbf{k}}-\hbar\omega}\delta(E_{c'\mathbf{k}'}-E_{v'\mathbf{k}'}-\hbar\omega)\left(\delta(E_{c\mathbf{k}}-E_{c'\mathbf{k}'}+\hbar\omega_{\mathbf{q}})+\delta(E_{v'\mathbf{k}'}-E_{v\mathbf{k}}+\hbar\omega_{\mathbf{q}})\right)\Bigg]\\ &+N_{\mathbf{q}}[\omega_{\mathbf{q}}\Leftrightarrow-\omega_{\mathbf{q}}]\Bigg\},\end{aligned} \tag{8}$$

where $\mathbf{q}=\mathbf{k}-\mathbf{k}'$ is the phonon momentum, $N_{\mathbf{q}}$ is the phonon population, and $[\omega_{\mathbf{q}}\Leftrightarrow-\omega_{\mathbf{q}}]$ denotes the term in brackets in Eq. (8) with instances of $\omega_{\mathbf{q}}$ negated, $\omega_{\mathbf{q}}$ being the phonon dispersion. The delta functions in Eq. (8) reflect the selection rule for optical transitions, and the electron-phonon coupling matrices together with principal parts modulate the transition rate. The initial asymmetric carrier distribution quickly thermalizes, so the carriers contribute to the current only for times on the order of the momentum relaxation time of the carriers, which is usually on the femtosecond timescale [25,27]. We approximate τ_0 to be 2 fs in this work, which is justified by an estimation from first-principles calculations (see Supplemental Material) [26,33,34]. Together, Eqs. (1) and (8) provide a method to compute the ballistic current density from quantities that are readily available from first-principles calculations.

We perform density functional theory (DFT) and density functional perturbation theory (DFPT) calculations using the QUANTUM ESPRESSO package [38,39]. Generalized gradient approximation exchange correlation functional and norm-conserving pseudopotentials produced by the OPIUM package are used [40–42]. The convergence threshold for self-consistent calculations was 10^{-8} Ry/cell, and for DFPT calculations it was 10^{-16} Ry/cell. Velocity and electron-phonon coupling matrices are calculated by Wannier interpolation using the EPW package [43,44]. All quantities are sampled on an $8\times8\times8$ unshifted Monkhorst-Pack grid [45], and the principal part integration is dealt with using a generalized Newton-Cotes method (see Supplemental Material) [33,35].

$BaTiO_3$, as a prototypical ferroelectric and bulk photovoltaic material, is an ideal candidate for benchmarking the ballistic current; the BPVE current spectrum has been measured for $BaTiO_3$ [28], and the shift current has also been predicted by first-principles calculations [7]. We use the experimental lattice parameters of tetragonal $BaTiO_3$ with Ti-displacement along (001) to represent the spatially averaged structure, and the atomic positions are relaxed before the phonon calculations. The temperature of phonons is chosen to be the room temperature. The theoretical ballistic current is shown in Fig. 2(a). We find that the ballistic current has a more jagged response profile, which is indicated by Ref. [20] as a signature of the ballistic current. For the range of light frequencies considered, the largest calculated response occurs at 2.1–2.5 eV above the band gap, similar to the shift current [Fig. 2(c)]. Even though the line shape of the ballistic current is more complicated, we note that the onset frequency of σ_{zzZ} is larger than that of σ_{xxZ} for both ballistic and shift current. In addition, the amplitudes of the ballistic and shift current are similar in magnitude, and thus we find that both shift current and ballistic current will contribute significantly to the experimentally measured current.

To compare with experiment, we calculate the real photocurrent based on the Glass coefficient [18,46], by further computing the absorption coefficient with quasiparticle corrections. As pointed out by our previous work [18], the quasiparticle correction will

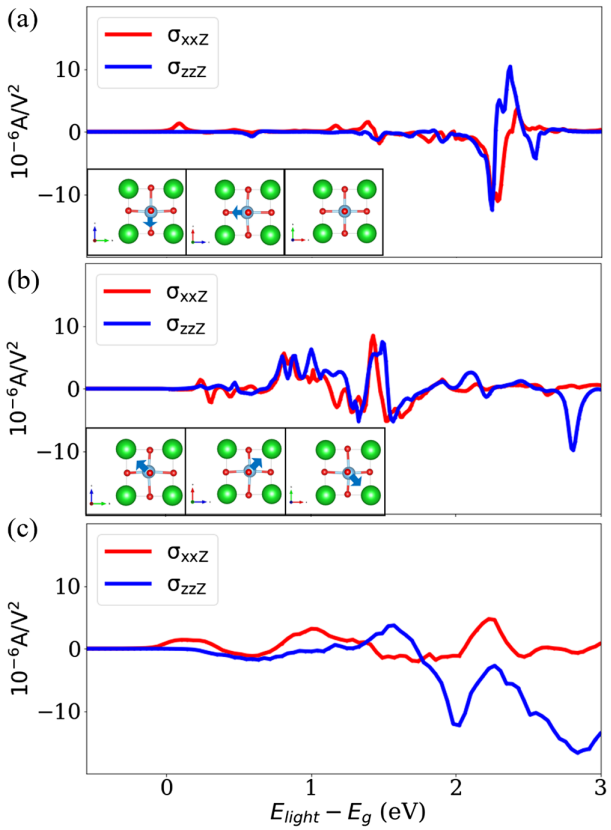

FIG. 2. First-principles results for $BaTiO_3$. (a) The ballistic current for the room-temperature tetragonal phase. (b) The ballistic current for the rhombohedral structure. (c) The shift current for the room-temperature tetragonal phase (reproduced from Ref. [7]). The insets of (a) and (b) show the structures of $BaTiO_3$ for each phase. It can be seen that the ballistic current and the shift current are of similar magnitude, and that structural change in $BaTiO_3$ can dramatically change the ballistic current response.

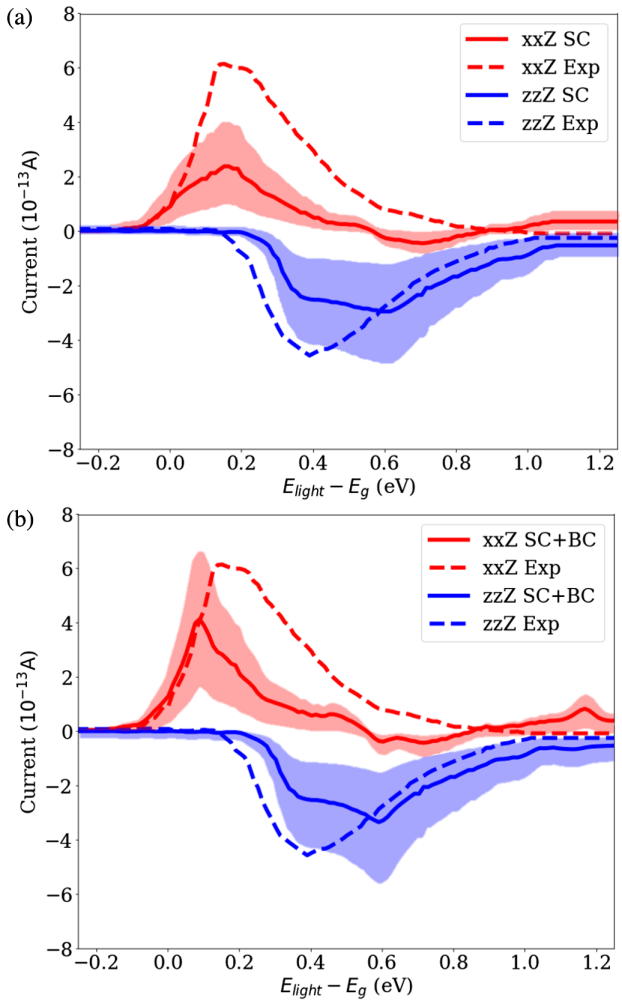

FIG. 3. Comparison between the theoretical and experimental results for tetragonal $BaTiO_3$ [18,28]. (a) The comparison between the experimental BPVE and the theoretical shift current (SC, reproduced from [18] with GW + exciton correction). (b) The comparison between the experimental BPVE and the theoretical shift current plus ballistic current (SC + BC). The solid lines are computed by assuming 0.5 mW/cm^2 light intensity and 0.15 cm sample width. The shaded areas account for the range of experimental parameters in Refs. [28,36] that gives the boundary of the response. For the xxZ component, the ballistic current partially fills the gap between the shift current and experimental spectra. For the zzZ component, the shift current alone agrees fairly closely with experiment, and the ballistic current barely influences the theoretical line shape.

significantly influence the absorption profile, but it will mainly blueshift the response tensor within the frequency range of interest. We apply the same technique by calculating the absorption coefficient using quasiparticle energies with exciton correction while calculating the current response tensor at the GGA level followed by a rigid shift to account for the underestimation of the band gap (2.1 eV at DFT-GGA level to 3.78 eV at quasiparticle level [18].) In this way, accuracy is improved while the computational cost is kept low. In addition, we consider the experimental errors for sample dimensions and light intensities as reported in Refs. [7,28,36]. In Fig. 3 the xxZ ballistic current partially fills the gap between the shift current and the experimental spectra, whereas for the zzZ component whose shift current has already aligned well with the experiments, the ballistic current barely influence the theoretical BPVE spectrum. This confirms that the ballistic current from the electron-phonon scattering can contribute significantly to the BPVE. However, we want to point out that in order to get a full understanding of the ballistic current and the BPVE, other scattering mechanisms such as defect scattering and electron-hole Coulomb scattering should also be taken into account.

As revealed by previous study, the shift current response can be strongly enhanced by modest changes to crystal structure or composition [47,48]. Here, we extend this idea

and explore the relation between the ballistic current and structure. We find that certain structures can greatly enhance the current response. To illustrate this point, we lift all constraints of $BaTiO_3$ and perform a full structural relaxation, so that the ground-state rhombohedral structure is obtained. In order to investigate the effect of crystal structure only, we then calculate its ballistic current by keeping the relaxation time and temperature unchanged, and the corresponding ballistic current photovoltaic tensor is shown in Fig. 2(b). Its line shape is dramatically different from that of the tetragonal phase [Fig. 2(a)], and the overall magnitude is much larger. Through a visual inspection of the two structures [the insets of Figs. 2(a) and 2(b)], we find a larger off-center displacement along the (111) direction in the rhombohedral structure and a smaller distortion along the (100) direction in the tetragonal phase. This could indicate a relation between the magnitudes of the current response and the structure distortion. Specifically, it could be that a larger extent of symmetry breaking will enhance the asymmetry of the momentum distribution, and the off-center displacement suggests that different parts of the Brillouin zone will not contribute to the ballistic current uniformly. A more quantitative investigation into the relationship between structure and the ballistic current will be the topic of our future study. For practical applications, however, this contrast between the ballistic current responses of rhombohedral and tetragonal $BaTiO_3$ is very illuminating since it shows that a large part of the solar spectrum can be harvested by engineering the distortion via doping or external strain.

In conclusion, based on the Kubo formula, we derived an expression for the phonon-assisted ballistic current, and we implement it in a first-principles calculation. Taking $BaTiO_3$ as an example we demonstrated via first-principles calculations that the electron-phonon coupling is an important mechanism of the ballistic current and can contribute significantly to the BPVE. We showed that, similar to the shift current, the ballistic current is also very sensitive to crystal structures; this reflects a promising possibility of material engineering to further harvest BPVE.

We acknowledge valuable discussions with Dr. Ruixiang Fei. This work was supported by the U.S. Department of Energy, Office of Science, Basic Energy Sciences, under Award No. DE-FG02-07ER46431. L. Z. T. was supported by the Molecular Foundry, a DOE Office of Science User Facility funded by the Office of Science of the U.S. Department of Energy under Contract No. DE-AC02-05CH11231. The analytical derivation was carried out by L. Z. T. and Z. D., and the numerical simulation was done by Z. D., A. M. S., and L. G. All research activities were supervised by A. M. R. Computational support was provided by the National Energy Research Scientific Computing Center (NERSC), a U.S. Department of Energy, Office of Science User Facility located at Lawrence Berkeley National Laboratory, operated under Contract No. DE-AC02-05CH11231.

*Corresponding author.
rappe@sas.upenn.edu
†These authors contributed equally to this work.

[1] V. I. Belinicher and B. I. Sturman, Sov. Phys. Usp. **23**, 199 (1980).
[2] R. von Baltz and W. Kraut, Phys. Rev. B **23**, 5590 (1981).
[3] W. Shockley and H. J. Queisser, J. Appl. Phys. **32**, 510 (1961).
[4] L. Z. Tan, F. Zheng, S. M. Young, F. Wang, S. Liu, and A. M. Rappe, npj Comput. Mater. **2**, 16026 (2016).
[5] J. E. Spanier, V. M. Fridkin, A. M. Rappe, A. R. Akbashev, A. Polemi, Y. Qi, Z. Gu, S. M. Young, C. J. Hawley, D. Imbrenda, G. Xiao, A. L. Bennett-Jackson, and C. L. Johnson, Nat. Photonics **10**, 611 (2016).
[6] J. E. Sipe and A. I. Shkrebtii, Phys. Rev. B **61**, 5337 (2000).
[7] S. M. Young and A. M. Rappe, Phys. Rev. Lett. **109**, 116601 (2012).
[8] J. Ibañez-Azpiroz, S. S. Tsirkin, and I. Souza, Phys. Rev. B **97**, 245143 (2018).
[9] C. Wang, X. Liu, L. Kang, B.-L. Gu, Y. Xu, and W. Duan, Phys. Rev. B **96**, 115147 (2017).
[10] T. Morimoto and N. Nagaosa, Sci. Adv. **2**, e1501524 (2016).
[11] Y. Zhang, F. de Juan, A. G. Grushin, C. Felser, and Y. Sun, Phys. Rev. B **100**, 245206 (2019).
[12] J. Ibañez-Azpiroz, I. Souza, and F. de Juan, Phys. Rev. Research **2**, 013263 (2020).
[13] J. A. Brehm, J. Mater. Chem. C **6**, 1470 (2018).
[14] T. Rangel, B. M. Fregoso, B. S. Mendoza, T. Morimoto, J. E. Moore, and J. B. Neaton, Phys. Rev. Lett. **119**, 067402 (2017).
[15] L. Z. Tan and A. M. Rappe, Phys. Rev. B **100**, 085102 (2019).
[16] B. M. Fregoso, T. Morimoto, and J. E. Moore, Phys. Rev. B **96**, 075421 (2017).
[17] A. M. Cook, B. M. Fregoso, F. De Juan, S. Coh, and J. E. Moore, Nat. Commun. **8**, 1 (2017).
[18] R. Fei, L. Z. Tan, and A. M. Rappe, Phys. Rev. B **101**, 045104 (2020).
[19] V. Belinicher and B. Sturman, Ferroelectrics **83**, 29 (1988).
[20] B. I. Sturman, Phys. Usp. **63**, 407 (2020).
[21] V. Alperovich, V. Belinicher, V. Novikov, and A. Terekhov, Ferroelectrics **45**, 1 (1982).
[22] H. T. Duc, C. Ngo, and T. Meier, Phys. Rev. B **100**, 045308 (2019).
[23] V. I. Shelest and M. V. Entin, Sov. Phys. Semicond. **13**, 1353 (1979).
[24] V. Belinicher and B. Sturman, Fiz. Tverd. Tela (Leningrad) **20**, 821 (1978).
[25] Z. Gu, D. Imbrenda, A. L. Bennett-Jackson, M. Falmbigl, A. Podpirka, T. C. Parker, D. Shreiber, M. P. Ivill, V. M. Fridkin, and J. E. Spanier, Phys. Rev. Lett. **118**, 096601 (2017).
[26] Y. Zhang, T. Holder, H. Ishizuka, F. de Juan, N. Nagaosa, C. Felser, and B. Yan, Nat. Commun. **10**, 1 (2019).

[27] A. M. Burger, R. Agarwal, A. Aprelev, E. Schruba, A. Gutierrez-Perez, V. M. Fridkin, and J. E. Spanier, Sci. Adv. **5**, eaau5588 (2019).
[28] W. Koch, R. Munser, W. Ruppel, and P. Würfel, Solid State Commun. **17**, 847 (1975).
[29] R. A. Jishi, *Feynman Diagram Techniques in Condensed Matter Physics* (Cambridge University Press, Cambridge, England, 2013).
[30] G. Giuliani and G. Vignale, *Quantum Theory of the Electron Liquid* (Cambridge University Press, Cambridge, England, 2005).
[31] G. D. Mahan, *Many-Particle Physics* (Springer Science & Business Media, New York, 2013).
[32] H. Fröhlich, Phys. Rev. **79**, 845 (1950).
[33] See Supplemental Material at http://link.aps.org/supplemental/10.1103/PhysRevLett.126.177403 for detailed analysis of diagrams, rationale for the choice of momentum relaxation time, preliminary discussion of the effect of temperature, and the generalized Newton-Cotes method, which includes Refs. [26,29,31,34–37].
[34] R. Fei, W. Song, and L. Yang, Phys. Rev. B **102**, 035440 (2020).
[35] L. Delves, Comput. J. (UK) **10**, 389 (1968).
[36] W. Koch, R. Munser, W. Ruppel, and P. Würfel, Ferroelectrics **13**, 305 (1976).
[37] J. Sjakste, K. Tanimura, G. Barbarino, L. Perfetti, and N. Vast, J. Phys. Condens. Matter **30**, 353001 (2018).
[38] P. Giannozzi, S. Baroni, N. Bonini, M. Calandra, R. Car, C. Cavazzoni, D. Ceresoli, G. L. Chiarotti, M. Cococcioni, I. Dabo *et al.*, J. Phys. Condens. Matter **21**, 395502 (2009).
[39] P. Giannozzi *et al.*, J. Phys. Condens. Matter **29**, 465901 (2017).
[40] J. P. Perdew, K. Burke, and M. Ernzerhof, Phys. Rev. Lett. **77**, 3865 (1996).
[41] A. M. Rappe, K. M. Rabe, E. Kaxiras, and J. D. Joannopoulos, Phys. Rev. B **41**, 1227 (1990).
[42] N. J. Ramer and A. M. Rappe, Phys. Rev. B **59**, 12471 (1999).
[43] F. Giustino, M. L. Cohen, and S. G. Louie, Phys. Rev. B **76**, 165108 (2007).
[44] S. Poncé, E. R. Margine, C. Verdi, and F. Giustino, Comput. Phys. Commun. **209**, 116 (2016).
[45] H. J. Monkhorst and J. D. Pack, Phys. Rev. B **13**, 5188 (1976).
[46] A. M. Glass, D. V. D. Linde, and T. J. Negran, Appl. Phys. Lett. **25**, 233 (1974).
[47] S.-J. Gong, F. Zheng, and A. M. Rappe, Phys. Rev. Lett. **121**, 017402 (2018).
[48] F. Wang, S. M. Young, F. Zheng, I. Grinberg, and A. M. Rappe, Nat. Commun. **7**, 10419 (2016).